Experimental Leak-Rate Measurement Through a Static Metal Seal

Christophe Marie, Didier Lasseux

Journal of Fluids Engineering, 2007, **129,** 799-805, DOI: 10.1115/1.2734250.

Experimental Leak-Rate Measurement Through a Static Metal Seal

This paper presents an experimental study to characterize fluid leakage through a rough metal contact. The focus is on an original experimental setup and procedure designed to measure the fluid micro (or nano) leak rate with great precision over several orders of magnitude. Liquid leak-rate measurements were carried out under two distinct operating conditions, i.e., in the case of a pressure gradient applied between contact edges and in the case of a pure diffusive effect resulting from a species concentration gradient. Experimental leak-rate results are discussed in terms of effective contact permeability—or transmissivity—and in terms of effective contact diffusivity versus contact tightening.

Keywords: seal, experiments, micro flow-rate measurement, gas phase chromatography, transmissivity, effective diffusivity

Christophe Marie
Département Génie Chimique,
IUT de l'Aisne, 48, rue d'Ostende,
02100 Saint-Quentin, France

Didier Lasseux[1]
Esplanade des Arts et Métiers,
Trefle (UMR CNRS 8508),
Site ENSAM,
33405 Talence Cedex, France
e-mail: didier.lasseux@bordeaux.ensam.fr

1 Introduction

Metal gaskets are commonly used for spatial and nuclear applications and, more generally, whenever severe thermodynamic conditions are met excluding the use of a rubber-sealant component. In such cases, the seal is performed by a direct-metal/metal-tight contact of rough surfaces for which many parameters controlling the leakage might be involved. Among others, one can cite the material of each surface, the topology at different scales of observation as a result of machining processes, the distribution and level of applied tightening, and the nature and thermodynamic state of the fluid to be sealed. Prediction and further optimization of the sealing efficiency of the contact are made difficult by (i) the identification of the relevant parameters and the way they can be controlled in contact design, (ii) the derivation of complete enough models able to correctly capture the physics of flow that can occur near the percolation threshold and of deformation which can be in the elastic and/or plastic regime [1], and (iii) last but not least, precise measurements of leak rate under well-controlled conditions for sometimes extremely small flow rates. The present paper is focused on this last issue since such measurements can be of interest with many respects.

In most reported experimental studies, seal performance of metal gaskets is investigated in very particular situations and generalization of leak rate results to other configurations or operating conditions has not been yet achieved. Most of the existing leak-rate measurements were performed with a gas and, to our knowledge, no direct comparison to liquid leakage was proposed in the literature in spite of some empirical relationship that justification still leaves much to be desired [2]. In fact, very few papers are reporting metal seal behavior with a detailed dependence of the leakage with the relevant parameters. An early contribution to this problem was proposed from a theoretical and experimental point of view in [3–5]. However, the reported work in these papers dealt with gas leakage in the free molecular regime through the contact between a rough surface and a perfectly flat and nondeformable plane while roughness distribution was assumed to be Gaussian. More recently, Yanagisawa et al. [6] studied the influence of tightening on gas leakage (air or helium), for a C seal from an experimental point of view only. The leak rate was measured using a "water bubble" method, but their investigation was limited to moderate loads because their maximum apparent contact pressure was roughly 200 MPa. Resulting deformations of the gasket under load and microscopic contact areas were also investigated, but no leak-rate predictions were proposed. In a subsequent work by the same authors [7] in 1991, the important role of a lead-coating layer was demonstrated from experiments at ambient and cryogenic temperatures (70 K) performed on C seals. During the same period, an experimental investigation on the influence of the type of machining on leakage was proposed by Matsuzaki and Kazamaki [8]. In their work, gas leak rates observed through contacts of turned, polished, and lapped surfaces made of different materials, such as copper, stainless steel, or other alloy steels were related to surface roughness and contact pressure. A nitrogen leak was detected using gas chromatography. Later, the same analysis was applied to the behavior of knife-edge seals [9], but no model was proposed to predict the leak.

From a theoretical and numerical point of view, some contact models of rough surfaces were reported recently in the literature. One can quote, for example, the numerical work of Kogut and Etsion [1] to describe the contact between a smooth rigid surface and a single asperity in the elastic-plastic domain. Such models, where no interaction between asperities is assumed along with no deformation of the substrate, had been also used before by Polycarpou and Etsion to predict an equivalent dimensionless aperture and gas leakage through the contact ([10,11]). This represents an interesting approach of leakage estimation although the simplified description of surface topology made by a Gaussian distribution of heights of asperities is quite far away from real surface finish frequently used and obtained by a turning process. Moreover, existing models are based on the hypothesis that leakage is mainly controlled by asperities, i.e., by microscopic defects on the surface. Complete studies in terms of scales of investigation (from the microscale to the entire contact scale) are necessary to improve the understanding of all the mechanisms controlling the leak and to capture the role of microscopic and macroscopic parameters. To this end, a complementary approach, consisting in accurate leakage measurements obtained under quasi-real but well-controlled conditions and, in particular, on real machined rough surfaces seems to be needed as pointed out in [12]. The experimental work reported in this paper is a first step to contribute to this task and is a starting point for subsequent comparison to models.

[1]Author to whom correspondence should be addressed.

Contributed by the Fluids Engineering Division of ASME for publication in the JOURNAL OF FLUIDS ENGINEERING. Manuscript received September 7, 2004; final manuscript received November 23, 2006. Review conducted by Joseph Katz.

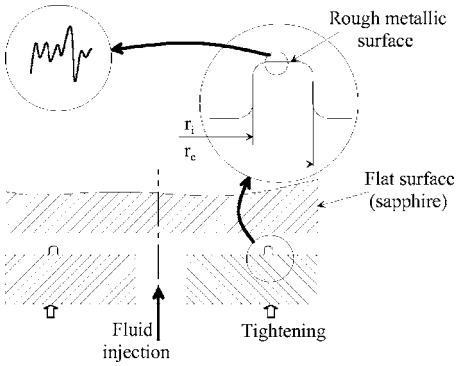

Fig. 1 Configuration of the contact under study

A precise and original method to measure leakage under well-defined conditions was designed and is presented below. It can be applied to flow-rate measurements ranging over six orders of magnitude in any configuration involving an annular contact between two rough surfaces and for both liquid and gas. The leak detection threshold is equivalent to that of mass spectrometry (i.e., typically 1 ppm), which represents a significant breakthrough for detection of a liquid flow rate. It is especially well adapted to measurements of very small flow rates expected for leak tests on systems requiring high sealing levels as well as in many other applications in the domain of microfluidics. In fact, many drawbacks of existing microliquid flow-rate devices are circumvented, such as sensitivity to temperature and/or pressure fluctuations, leakage, evaporation, etc. [13]. An experimental setup using this method was developed, and leak-rate measurements were performed under well-defined conditions on a model configuration close to a real design. Flow rates measured on the entire contact are analyzed in terms of the macroscopic properties of the assembly versus contact pressure. These macroscopic properties are the *effective transmissivity* and *effective diffusivity* and are direct signatures of the connected aperture field, i.e., of interconnected zones of no local effective contact between the two surfaces. These experimental results will serve as a basis for further comparison to predictive estimates of leakage obtained from topological analysis of the surfaces along with numerical simulation of deformation and flow through the contact. A detailed presentation of such a comparison, which is beyond the scope of this paper, will be reported later on. Here, we lay the emphasis upon the methodology which reveals to be very effective.

Section 2 of this paper is dedicated to the description of the experimental apparatus used to perform leak-rate measurements. Results obtained for liquid leakage are presented in Sec. 3. For both pressure-driven and diffusive flows, results were obtained while varying tightening applied to the assembly as well as liquid pressure in the case of viscous flows.

2 Experimental Setup

2.1 Contact Configuration. The configuration for seal tests investigated in the experiments presented below is that of a plane annular and circular contact between a machined metallic surface obtained by turning and made of 316L stainless steel pressed against the plane cross section of a cylinder made of sapphire as schematically represented in Fig. 1. The turning process generates defects ranging from the microscale (metallic grain scale) to the macroscale (error of forms at the scale of the entire contact) [14].

The ring-shaped contact has an inner radius r_i of 19.85 mm and an outer radius r_e of 20.15 mm, yielding an apparent contact area of 38 mm^2. Two surfaces, referred to as A and B and obtained in very different machining conditions, were used in our experiments. Parameters used for the machining of surface B are reported in Table 1.

Table 1 Turning parameters used for metallic surfaces B

Speed	1200 rpm
Advance by turn	0.05 mm
Depth of cut	0.02 mm
Turning tool	45 deg
Tool radius	0.2 mm

Our objective here is not to mimic metal/metal contact as employed in real configurations but rather to acquire data under simple but well-controlled conditions in the perspective of direct comparison to models. Within this context, a sapphire was chosen for the antagonist and this was motivated by several reasons. First, this allows great simplifications in the description of the contact topology tractable for future use in predictive tools. Indeed, polished surfaces as well as excellent flatness properties can be obtained on the sapphire. Moreover, hardness and Young's moduli ratios between the sapphire and 316 L stainless steel are roughly 10 and 2, respectively, as indicated in Table 2. Under these circumstances, the sapphire can be considered as a flat nondeformable surface; thus, the topological and mechanical properties of the contact are those of the metallic surface only. In other words, this configuration is an excellent experimental support for a straightforward description of the contact with the surface-sum concept without ambiguity. This concept, first introduced in [15], was later confirmed as a relevant one in several works [16–18]. Second, transparency will allow direct visualization of the contact for future study. Of course, the experimental device can be used with any pair of materials and other dimensions of the contact.

2.2 Experimental Device. The experimental setup used in this work is schematically represented in Fig. 2 [19]. It consists of a very rigid leakage cell designed to contain and support the different parts of the contact. Within the leakage cell, the metallic rough surface is pressed against the sapphire disk using a jack

Table 2 Mechanical properties of stainless steel and sapphire used in the experiments

	316L stainless steel	Sapphire
Vickers Hardness	155–190	1570–1750
Young's modulus	1.9×10^5–2.1×10^5 MPa	4.4×10^5 MPa
Tensile strength	460–860 MPa	190 MPa
Poisson's ratio	0.3	0.3
Compressive strength	-	2100 MPa

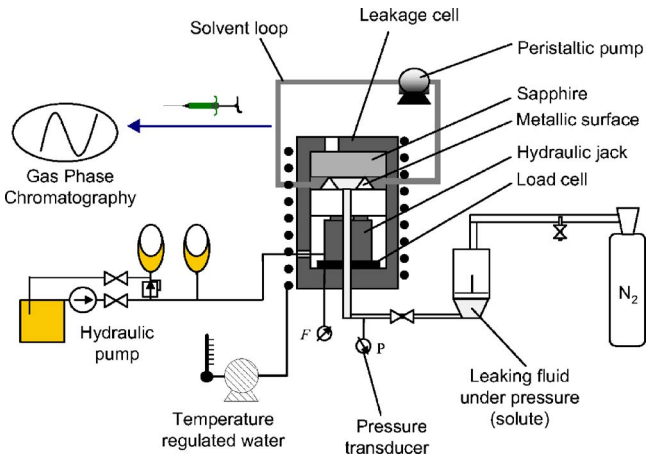

Fig. 2 Schematic representation of the experimental apparatus (viscous flow conditions)

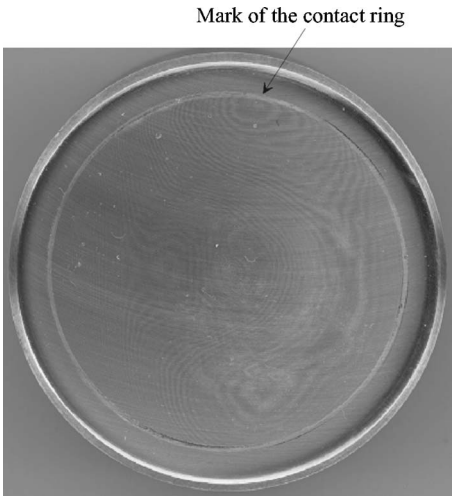

Fig. 3 Indentation of a polished copper surface by the rough metallic ring, P_{ca}=50 MPa

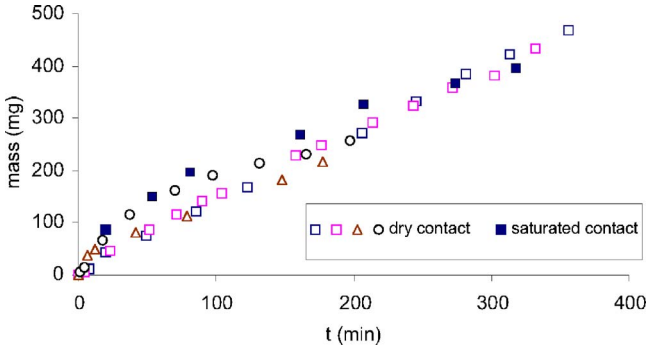

Fig. 4 Mass of leaking fluid through the contact versus time - P_{ca}=240 MPa - ΔP=9 bar. Open and dark symbols correspond to an initial dry and wet contact respectively

connected to a hydraulic pump. Tightening is controlled by a load cell made of a gage bridge sensor, ensuring a continuous measurement during experiments. From this measurement, the apparent contact pressure, referred to as P_{ca} in the rest of this work is defined as the nominal force F, divided by the apparent contact area

$$P_{ca} = \frac{F}{\pi(r_i^2 - r_e^2)} \tag{1}$$

The leakage cell is kept at 20°C during experiments using a coil in which temperature regulated water flows.

Excessive care was taken to avoid out of parallelism errors between the metallic surface and the sapphire by introducing a ring of soft material (rubber or polytetrafluoroethylene) above the sapphire cylinder and below the metallic surface. Because these materials are far less rigid than both the metal and sapphire and since their Poisson's ratio are close to 0.5, they behave like a fluid ball-and-socket joint and ensure an excellent correction of this error. This was verified with a test experiment where the sapphire disk was replaced by a copper cylinder while a 50 MPa contact pressure was applied. As sketched on Fig. 3, the mark corresponding to the ring indentation of the 316L surface on the polished copper face is extremely regular excluding any significant deflection between the metallic surface and the sapphire.

The liquid for which leakage is measured is stored in a tank axially connected to the inner part of the contact and may be put under pressure using nitrogen. The pressurized liquid—or solute—leaks through the contact and is collected in a closed loop of solvent. Circulation of the solvent loop is necessary to improve homogeneity of the mixture and is carried out with a peristaltic pump. It is kept slow enough to avoid a significant pressure gradient in the outer part of the contact, which is supposed to remain at the atmospheric pressure. Leak-rate measurements are performed by measuring the mass of solute passing through the contact in the solvent, during a given period of time. This is achieved by sampling the solvent loop, regularly, taking 1 μl from the mixture with a microsyringe. The sample is analyzed by gas phase chromatography (GPC) providing the solute concentration.

For experiments under diffusive conditions, the setup is modified by simply replacing the nitrogen and liquid storage tanks by a U tube containing the liquid for which leakage is measured. One end of the tube is connected to the inner region of the contact while the other end is left opened, the liquid level being adjusted at the height of the metal/sapphire contact so that no pressure difference exists between contact edges.

In our experiments, the fluid for which the leak rate was measured is 1-butanol while the collector solvent is ethanol. These alcohols were strongly wetting both metal and sapphire surfaces in the presence of air. Accuracy of leak-rate measurement was improved significantly by adding an internal standard (1-propanol) to the solvent, and using calibration performed prior to experiments [20]. Chromatograms were recorded by making use of a flame ionization detector. This technique ensures a rapid, accurate, and high sensitive measurement and has an excellent compatibility with the alcohols used in our experiments.

Experimental results reported below were obtained with a tightening ranging from 3.8 kN to 30.4 kN. This corresponds to an apparent contact pressure (P_{ca}) between 100 and 800 MPa. During pressure-driven experiments, the pressure difference, ΔP, between the solute in the inner region of the contact and the solvent in the loop (remaining roughly at atmospheric pressure) ranged from 1 to 30 bar and was measured using a pressure transducer with a precision of 60 mbar.

2.3 Experimental Protocol. Leak-rate measurements were carried out every P_{ca} increment of 100 MPa from low to high tightening. This procedure avoids possible roughness plastic deformation at high loads that might otherwise remain during measurements at lower loads. Because expected leak rates are extremely small (sometimes <1 μg/min), special attention must be addressed to the experimental protocol. For instance, excessive care must be taken of surfaces cleanness since trapped or adsorbed solute might be slowly solubilized in the solvent loop and might be a source of significant error while estimating the leak rate.

For the initial state, two different configurations of the contact may be considered. In fact, the contact can be first wetted and saturated with the leaking fluid before load is applied or the experiment can be started with a dry contact. The former case would ensure leakage under the one-phase flow condition, whereas in the later, a leak initiates under the two-phase flow condition at least during a short period during which the contact is partially saturated by air and is being invaded by imbibition. Tests were performed to explore both cases. As shown in Fig. 4, no significant effects were noted between the two situations and, for simplicity reasons regarding cleanness, experiments were started with a dry contact.

After pressure was applied in the solute during pressure-driven experiments, the resulting force exerted on the sapphire and the metallic surface, which tends to unload the contact, was corrected by increasing the tightening of the corresponding value. Once both pressure in the fluid phase and tightening reached stabilized values, the solvent loop was analyzed by GPC at regular intervals of time. This provides the time evolution of the mass of butanol leaking through the contact.

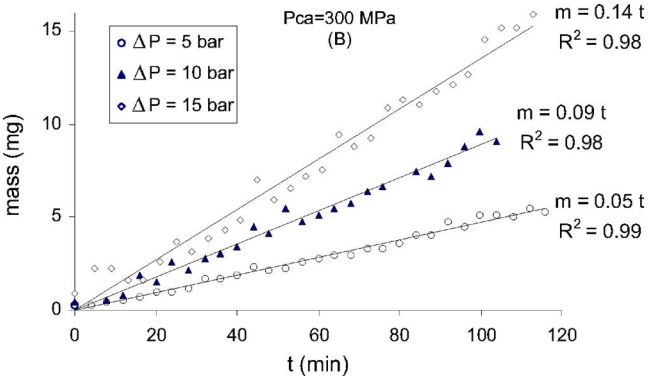

Fig. 5 Time evolution of the mass of butanol in the solvent loop - Surface B1

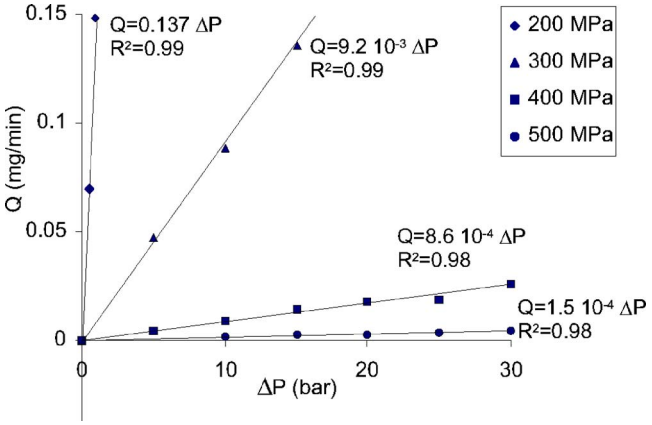

Fig. 7 Mass leak-rate versus pressure drop through the contact for four values of tightening - Surafce B1

3 Experimental Results

In this section, we report some results of leak-rate measurements performed during experiments under viscous and diffusive conditions. In both cases, the leak rate was recorded while varying the apparent contact pressure P_{ca} and the pressure difference between contact edges during viscous flow experiments. As mentioned above, two different types of surfaces—A and B—were used in these experiments. Moreover, two surfaces of type B (i.e., B1 and B2) obtained under the same machining conditions were employed for comparison purposes.

3.1 Leak-Rate Measurements Under Pressure-Driven Conditions. In Fig. 5, we have represented the time evolution of the mass of butanol leaking through the contact between the sapphire and the metallic surface B1, for three different values (5 bar, 10 bar, and 15 bar) of the pressure difference ΔP. Experimental results reported in Fig. 5 were obtained with an apparent contact pressure equal to 300 MPa. Measurements were performed over roughly 100 min.

As can be seen in Fig. 5, the mass of butanol present in the solvent loop evolves linearly versus time and we shall insist on the excellent values of the associated determination coefficient [21]. This linear evolution is confirmed on similar results obtained on surface A and reported in Fig. 6, indicating moreover an excellent reproducibility between two measurements performed under identical conditions without dismantling between two successive experiments [22].

As expected, the leak can be characterized by a unique value of the mass flow rate for each value of both the apparent contact pressure and pressure drop between contact edges. The experimental value of this flow rate can be clearly extracted from the slope of trend lines issued from $m(t)$ data illustrated above using a least-squares linear fit approach. By doing so, we assume that the error on the measurement of $m(t)$ remains the same at any time so that the optimal estimation of the flow rate is, in fact, that resulting from a linear least-squares approach. Results of this procedure applied to data obtained on surface B1 are depicted in Fig. 7, where we have represented the mass leak rate Q versus pressure drop for four values of the apparent contact pressure.

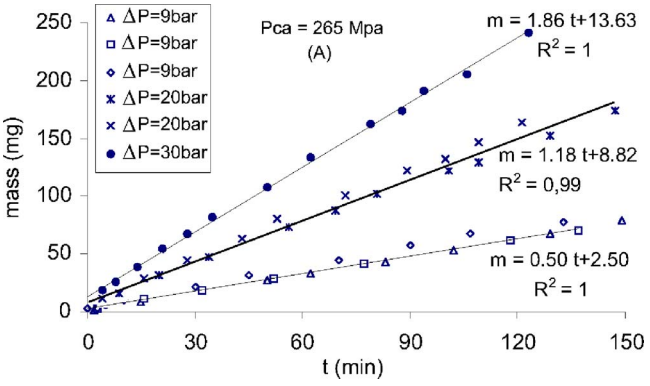

Fig. 6 Time evolution of the mass of butanol in the solvent loop - Surface A

Again, as expected, one can observe that the mass leak rate depends linearly on the pressure drop with excellent determination coefficients. In addition, the method used in the present work turns out to be extremely sensitive to detect liquid leakage and is actually as sensitive as mass spectrometry classically used for gas leak detection [2,23,24]. In fact, leak rates as weak as 10^{-4} mg/min can be measured with the system used in the present work and this can be achieved by increasing the period of observation and, eventually, by reducing the volume of the solvent loop. Examples of results in this range of leak rate obtained on surface B2 for P_{ca} equal to 700 MPa and fluid pressure drops equal to 10 bar, 20 bar, and 30 bar respectively are reported in Fig. 8.

One can note, in Fig. 8, that butanol was initially introduced in the solvent loop so that this species is initially above the chromatograph detection threshold. Here, the noise is very significant compared to the amount of solute collected in the loop and this leads to small values of the determination coefficients. Nevertheless, in the particular case of a linear regression, one can approximate the variance, $\mathrm{Var}(\mathsf{Q})$, on the estimator of the mass leak rate (i.e., on the slope of the trend line issued from $m(t)$ data). This variance is given by

$$\mathrm{Var}(\mathsf{Q}) = \frac{1}{(n-1)} \frac{\sum (Y^{\mathrm{model}} - Y)^2}{\sum X^2} \tag{2}$$

where n is the number of $Y(X)$ measurements, Y being the mass of butanol measured at time X and Y^{model}, representing the mass of butanol estimated at time X from the trend line equation [25]. For measurements reported in Fig. 8, this leads to standard deviations $<14\%$ for $\Delta P=10$ bar, 10% for $\Delta P=20$ bar, and 5% for $\Delta P=30$ bar. These very low flow rates obtained for $P_{ca}=700$ MPa on surface B2 are represented versus ΔP in Fig. 9, where, again, an excellent linear relationship can be observed along with a zero flow rate for a zero pressure drop.

The linearity between mass leak rate and pressure drop allows a description of the flow through the contact by a macroscopic Reynolds law classically used for flow in fractures [26,27], which, for the ring-shaped contact under study, can be written under the form

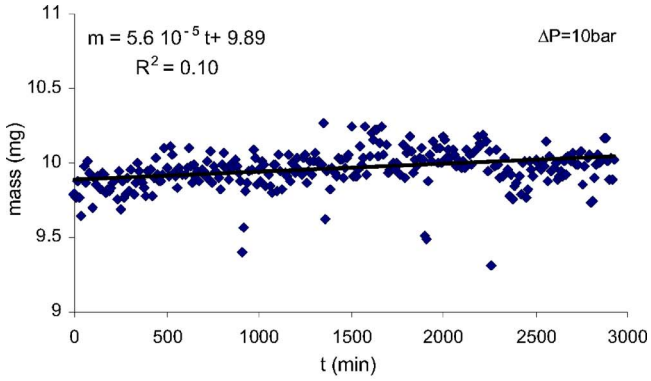

(*a*)

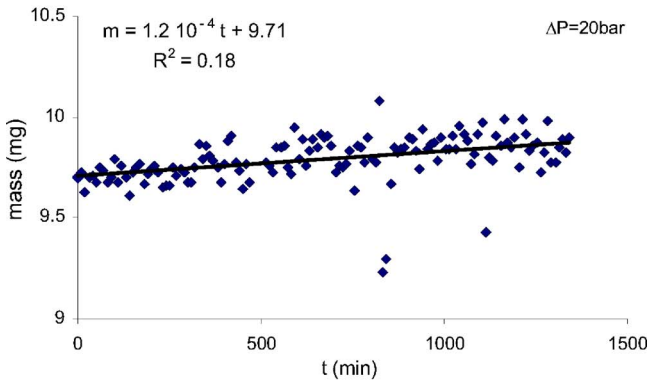

(*b*)

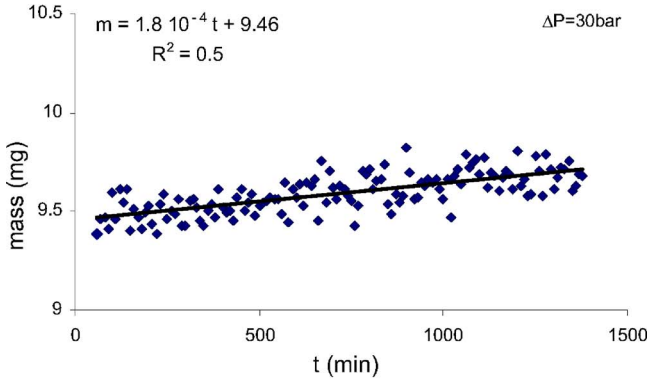

(*c*)

Fig. 8 Time evolution of the mass of butanol in the solvent loop - Surface B2 - P_{ca}=700 MPa - a) ΔP=10 bars - b) ΔP =20 bars - c) ΔP=30 bars

$$\frac{Q}{2\pi} = \rho \frac{K}{\mu} \frac{\Delta P}{\ln(r_e/r_i)} \tag{3}$$

In this relationship, r_e and r_i are the external and internal radii of the contact, μ is the dynamic viscosity of the leaking fluid (for butanol at 20°C, $\mu = 2.95 \times 10^{-3}$ Pa s) and ρ is the density of butanol (ρ=810 kg/m^3 at 20°C) considered as an incompressible phase in the pressure range investigated in these experiments, and K is the contact transmissivity having the unit of cubic meters. It must be emphasized that, from an engineering point of view, K is a key parameter since it is an intrinsic characteristic of the contact at a given P_{ca} and should be used to qualify sealing efficiency. By making use of Eq. (3), one can easily estimate the transmissivity of the contact from slopes of trend lines of $Q(\Delta P)$ data for each value of P_{ca} using again a least-squares linear fit approach if one

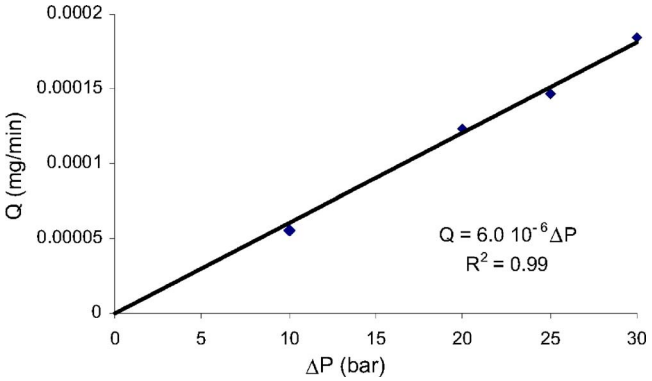

Fig. 9 Mass leak-rate versus pressure drop - P_{ca}=700 MPa - Surface B2

assumes a constant error on $Q(\Delta P)$. In Fig. 10, we have represented the evolution of transmissivity obtained on surfaces B1 and B2 versus the apparent contact pressure. Estimations of the corresponding errors are provided in Sec. 3.

These results clearly highlight the strong dependence of sealing efficiency on tightening. In fact, transmissivity varies over approximately seven orders of magnitude while the apparent contact pressure varies between 100 MPa and 700 MPa. As shown in Fig. 11, the evolution seems to roughly obey a power law and fits performed on our experimental data indicate that K can be scaled as

$$K \propto P_{ca}^{-6.4} \tag{4}$$

for surface B1 and

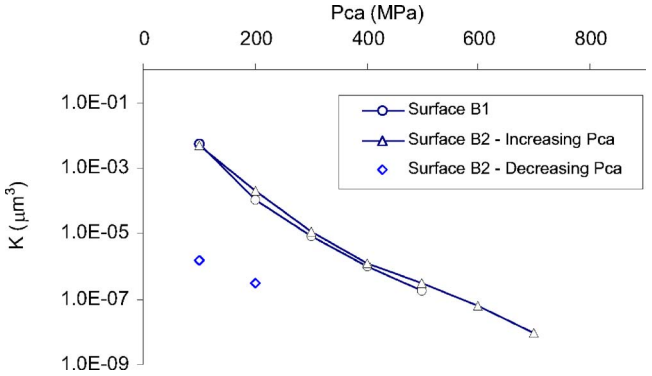

Fig. 10 Contact transmissivity versus tightening for two similar rough surfaces B1 and B2

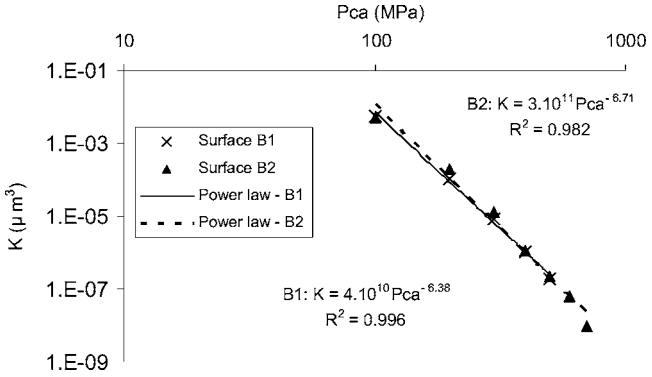

Fig. 11 Power law fits on K(P_{ca}) - Surfaces B1 and B2

$$\mathsf{K} \propto P_{ca}^{-6.7} \tag{5}$$

for surface B2.

No leak was detected for $P_{ca} > 800$ MPa on surface B2, and after this value of P_{ca} has been reached and tightening is decreased, a completely different behavior of transmissivity is observed since at 200 MPa and 100 MPa leak rates are respectively divided by a factor 700 and 2400. This hysteresis must be the proof of permanent deformations of surface defects in the plastic domain remaining during the contact pressure release.

As shown in Fig. 10, transmissivities for both surfaces are very similar over the range of apparent contact pressure investigated here. However, as will be seen below with results obtained on effective diffusivities, it is not sufficient to conclude that aperture fields are completely similar. This can be explained by the fact that viscous flow explores a complex average operating on the cube of the aperture field whereas diffusive flux is related to another average formed on the aperture field only [28]. As said before, a direct comparison of these experimental data to a theoretical and numerical analysis of both surface deformation and flow within the aperture field will be reported later on.

3.2 Leak-Rate Measurements Under Diffusive Operating Conditions. Experiments described in this section aim at the determination of solute mass flux through the contact resulting from a diffusion process due to the concentration gradient of chemical species between contact edges without any pressure gradient. This type of experiment is motivated by the fact that a diffusive leak provides a signature of the aperture field, which differs from that revealed by viscous leak. In these experiments, we only consider the flux of butanol contained inside the contact into ethanol (and propanol) contained in the solvent loop. Diffusive leak-rate measurements were carried out on surfaces B1 and B2 while, as for viscous leak rate measurements, contact pressure was varied between 100 MPa and 800 MPa. Because fluxes are extremely small and close to the chromatography detection threshold, measurements were performed over large periods of time (typically several hundreds of hours).

If the aperture field is slowly varying all over the contact, i.e., if the local slope on the rough surface everywhere is small compared to unity, it can be easily shown by integration of a classical Fick's law that the diffusive mass flux Q_d (here, butanol in ethanol) is given by a relation similar to Eq. (3)

$$\frac{\mathrm{Q}_d}{2\pi} = \mathrm{D}_{\mathrm{eff}} \frac{(c_i - c_e)}{\ln(r_e/r_i)} \tag{6}$$

In Eq. (6), r_e and r_i are the external and internal radii of the contact, c_e and c_i are the external and internal mass concentrations of the leaking fluid (butanol), and $\mathrm{D}_{\mathrm{eff}}$ the effective "diffusivity" of the contact (in cubic meters per second). If one assumes that c_e remains extremely small ($c_e \approx 0$) in the solvent loop and that the inverse flux of ethanol (and propanol) is negligible, an alternate form of Eq. (6) is

$$\frac{\mathrm{Q}_d}{2\pi} = \mathrm{D}_{\mathrm{eff}} \frac{\rho}{\ln(r_e/r_i)} \tag{7}$$

where ρ is the density of butanol.

Our experimental results of diffusive mass leak rate measurement were used in Eq. (7) to identify $\mathrm{D}_{\mathrm{eff}}$ following the same procedure as the one used to determine K. In Fig. 12, we have represented the ratio $\mathrm{D}_{\mathrm{eff}}/D$ versus P_{ca}, D being the molecular diffusion coefficient of butanol in ethanol. Here, we took $D = 10^{-9}$ m^2/s. It should be emphasized that, as for K, $\mathrm{D}_{\mathrm{eff}}/D$ is an intrinsic property of the contact which only depends on the aperture field topology for a given P_{ca}.

No leak rate was detected at 300 MPa on surface B1, and at 500 MPa on surface B2. As can be observed on results on surface B2, effective diffusivity strongly decreases over roughly four orders of magnitude when tightening increases from 100 MPa to 400 MPa. Moreover, the values of $\mathrm{D}_{\mathrm{eff}}$ significantly differ between the two surfaces although transmissivities were very similar.

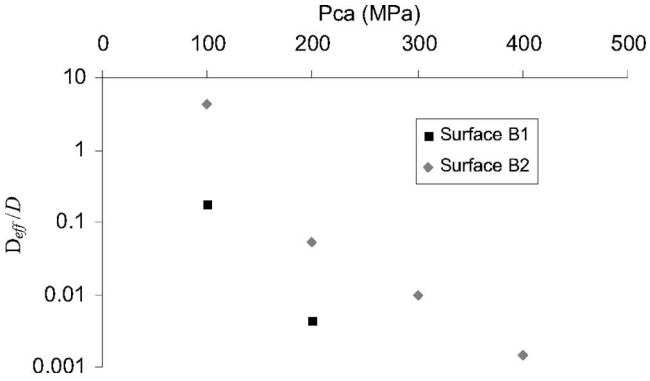

Fig. 12 Ratio of effective diffusivity to molecular diffusion coefficient determined from experimental leak rate measurements - Surfaces B1 and B2

3.3 Measurements Uncertainty. Global uncertainty on transmissivity and effective diffusivity can be expressed in a simplified manner as

$$\frac{\Delta \mathsf{K}}{\mathsf{K}} = \frac{\Delta \mathsf{Q}}{\mathsf{Q}} + \frac{\Delta \mu}{\mu} + \frac{\Delta(\Delta P)}{\Delta P} + \frac{\Delta r}{\ln(r_e/r_i)}\left(\frac{1}{r_e} + \frac{1}{r_i}\right) \tag{8}$$

$$\frac{\Delta \mathrm{D}_{\mathrm{eff}}}{\mathrm{D}_{\mathrm{eff}}} = \frac{\Delta \mathrm{Q}_d}{\mathrm{Q}_d} + \frac{\Delta r}{\ln(r_e/r_i)}\left(\frac{1}{r_e} + \frac{1}{r_i}\right) \tag{9}$$

where no error was assumed on ρ. The corresponding value of tightening must also be considered with its own uncertainty

$$\frac{\Delta P_{ca}}{P_{ca}} = \frac{\Delta F}{F} + \frac{2\Delta r}{r_e - r_i} \tag{10}$$

keeping in mind that these three last expressions are actually *overestimations* of the relative errors.

In Eqs. (8) and (9), $\Delta\mathsf{Q}$ and $\Delta \mathrm{Q}_d$ were simply approximated by the mean values of the standard deviations given by Eq. (2) on all the values of Q and Q_d used to estimate K and $\mathrm{D}_{\mathrm{eff}}$, respectively. The term $\Delta\mu/\mu$ in Eq. (8) results from temperature fluctuations, and we estimated this relative error to 0.25%. This corresponds to the viscosity variation of butanol at 20°C due to a temperature fluctuation of 0.1°C. The error on ΔP results from measurement accuracy performed with the pressure transducer and is equal to 60 mbar. To account for fluctuations over time due to microleakage in the nitrogen circuit, we also took a relative error of 1% on ΔP. The contribution of the pressure drop error on $\Delta\mathsf{K}/\mathsf{K}$ in Eq. (8) was taken as the average value of all the values of $\Delta(\Delta P)/\Delta P$ used to determine K. As for ΔP, the error on F results from the measurement with the load cell which accuracy is 75 N as well as fluctuations over time due to microleakage in the hydraulic circuit of the jack and we took $\Delta F/F$ equal to 1% to account for this. It must be noted that ΔP and F are coupled parameters since solute pressure variations induce tightening fluctuations. However, coupling was not considered in the present estimation. Finally, for the error on the external and internal radii of the contact ring, we took

$$\Delta r_e = \Delta r_i = \Delta r = 0.01 \text{ mm} \tag{11}$$

As an illustration, estimations of the relative errors on P_{ca} and on experimental results obtained for K and $\mathrm{D}_{\mathrm{eff}}$ on surface B2 are reported in Table 3.

One can see on these results that the relative error on P_{ca} is $<10\%$ and slightly decreases while increasing the load. This is due to the fact that $\Delta F/F$ decreases, whereas the major contribu-

Table 3 Uncertainties on P_{ca} transmissivities, and effective diffusivities obtained on surface B2

P_{ca} (MPa)	$\frac{\Delta P_{ca}}{P_{ca}}$ (%)	$\frac{\Delta K}{K}$ (%)	$\frac{\Delta D_{eff}}{D_{eff}}$ (%)
100	9.7	15	7
200	8.7	15	7
300	8.3	10	8
400	8.2	11	16
500	8.1	10	
600	8.0	11	
700	8.0	19	

tion, which comes from the term involving Δr, remains constant. For K, the relative error is large for small values of P_{ca}, decreases for moderate loads and increases again for larger values of P_{ca}. In fact, for small values of P_{ca}, leak rate measurements require small values of ΔP for which relative errors are very significant. For large values of P_{ca}, flow rates are very small and the relative error on Q is the major contribution to $\Delta K/K$. In the same manner, the relative error on D_{eff} increases with P_{ca} due to the increase of $\Delta Q_d/Q_d$.

4 Conclusion

In this work, an original experimental method and device were designed and used to measure leak rate through a metal contact seal. The experimental technique allows measurements of liquid mass flow rates as small as 10^{-4} mg/min with great precision under well-controlled conditions of temperature, pressure in the fluid to be sealed, and tightening (i.e., apparent pressure) applied to the contact. Here, a uniform apparent contact pressure P_{ca} was considered. The technique reveals to be as sensitive as mass spectrometry classically employed for gas leak-rate measurements, and this represents a significant breakthrough in comparison to existing methods. Although any other configuration could be used, experiments were performed on a model contact between a plane metallic ring obtained by turning and a sapphire surface. This choice was motivated by the fact that the topology of the contact can be described in this case by that of the metallic surface only, which will significantly simplify future comparison to predictive models. Because of the sensitivity of the method, the leak was investigated in the rather classical viscous flow regime but also in the pure diffusive regime resulting from a species gradient.

As expected, experimental results reproduce linear dependence of the flow rate on the driving force (i.e., the pressure or concentration gradient) and excellent correlation coefficients are obtained. The linear dependence provides the *transmissivity*, K in the viscous case and the *effective diffusivity* D_{eff}, in the diffusive case. These coefficients are the macroscopic characteristics of the whole contact essential for engineering purposes. Because they explore two different averages of the aperture field, K and D_{eff}/D provide interesting complementary data on the contact behavior regarding seal efficiency. Experimental results indicate that, in the configuration under study, these coefficients vary very strongly with the apparent contact pressure following stiff power laws (K decreases over roughly six orders of magnitude in the range of 100–800 MPa for P_{ca}). The methodology developed in the present study, coupled to deformation and flow descriptions with appropriate models along with topological analysis at different scales of observation, should contribute to understand (and further improve) seal behavior under very different operating conditions.

Use of this experimental technique can also be interesting in many other domains of the microfluidic whenever very small liquid flow rates are to be accurately measured or controlled.

Acknowledgment

This work was performed within the framework of a group of research including CNRS, CNES, EDF, and SNECMA from which financial support is gratefully acknowledged. We also thank G. Carillon for his help.

References

[1] Kogut, L., and Etsion, I., 2003, "A Finite Element Based Elastic-Plastic Model for the Contact of Rough Surfaces," Tribol. Trans., **46**(3) pp. 383–390.

[2] Amesz, J., 1966, "Conversion of Leak Flow-Rates for Various Fluids and Different Pressure Conditions," Report of the ORGEL program, European Atomic Energy Community—EURATOM, EUR2982.e.

[3] Armand, G., Lapujoulade, J., and Paigne, J., 1964, "A Theoretical and Experimental Relationship Between the Leakage of Gases Through the Interface of Two Metals in Contact and Their Superficial Micro-Geometry," Vacuum, **14**(2), pp. 53–57.

[4] Armand, G., and Lejay, Y., 1967, "Déformation des microgéométries de surfaces planes en contact: Application à l'écoulement gazeux interfacial (cas des déformations plastiques)," Rev. Fr. Méc., **21**, pp. 15–29.

[5] Lejay, Y., 1967, "Déformation des microgéométries de surfaces planes en contact: Application à l'écoulement gazeux interfacial (cas du recouvrement élastique)," Rev. Fr. Méc., **21**, pp. 31–40.

[6] Yanagisawa, T., Sanada, M., Koga, T., and Hirabayashi, H., 1990, "Fundamental Study of the Sealing Performance of a C-Shaped Metal Seal," *2nd International Symposium on Fluid Sealing*, La Baule, Sep. 18–20, pp. 389–398.

[7] Yanagisawa, T., Sanada, M., Koga, T., and Hirabayashi, H., 1991, "The Influence of Designing Factors on the Sealing Performance of C-Seal, SAE Trans., **100**(6), pp. 651–657.

[8] Matsuzaki, Y., and Kazamaki, T., 1988, "Effect of Surface Roughness on Compressive Stress of Static Seals, JSME Int. J., Ser. III, **31**, pp. 99–106.

[9] Matsuzaki, Y., Hosokawa, K., and Funabashi, K., 1992, "Effect of Surface Roughness on Contact Pressure of Static Seals," JSME Int. J., Ser. III, **35**, pp. 470–476.

[10] Polycarpou, A. A., and Etsion, I., 1998, "Static Sealing Performance of Gas Mechanical Seals Including Surface Roughness and Rarefaction Effects," Tribol. Trans., **41**(4) pp. 531–536.

[11] Polycarpou, A. A., and Etsion, I., 2000, "A Model for the Static Sealing Performance of Compliant Metallic Gas Seals Including Surface Roughness and Rarefaction Effects, Tribol. Trans., **43**(2) pp. 237–244.

[12] Etsion, I., and Front, I., 1994, "A Model for Static Sealing Performance of End Face Seals," Tribol. Trans., **37**(1) pp. 111–119.

[13] Colin, S., 2004, *Microfluidique*, Lavoisier, Paris.

[14] Rakhit, A. K., Sankar, T. S., and Osman, M. O. M., 1976, "The Influence of Metal Cutting Forces on the Formation of Surface Texture in Turning," Int. J. Mach. Tool Des. Res., **16**(4), pp. 281–292.

[15] Greenwood, J. A., and Tripp, J. H., 1970, "The Contact of Two Nominally Flat Rough Surfaces," Proc. Inst. Mech. Eng., **71**(185), pp. 48–71.

[16] O'Callaghan, P. W., and Probert, S. D., 1987, "Prediction and Measurement of True Areas of Contact Between Solids, Wear, **120**, pp. 29–46.

[17] Francis, H. A., 1977, "Application of Spherical Indentation Mechanics to Reversible and Irreversible Contact Between Rough Surfaces," Wear, **45**, pp. 221–269.

[18] McCool, J. L., 1985, "Comparison of Models for the Contact of Rough Surfaces," Wear, **107**, pp. 37–60.

[19] Marie, C., 2002, "Fuite monophasique au travers d'un contact rugueux: Contribution à l'étude de l'étanchéité statique," Ph.D. thesis, Université Bordeaux 1.

[20] Tranchant, J., 1995, *Manuel pratique de chromatographie en phase gazeuse*, 4th ed., Masson, Paris.

[21] Marie, C., and Lasseux, D., 2001, "Analyse expérimentale d'une fuite liquide au travers d'un contact statique métal/métal," 15ème Congrès Français de Mécanique, Nancy, Sep. 3–7.

[22] Marie, C., and Lasseux, D., (2002), "Fuite monophasique dans un contact rugueux," Journées CNES Jeunes Chercheurs, Centre Spatial de Toulouse, Apr. 24–26, pp. 138–139.

[23] Pregelj, A., Drab, M., and Mozetic, M., 1997, "Leak Detection Methods and Defining the Size of Leaks", The 4th International Conference of Slovenian Society for Non Destructive Testing, Ljubljana, Slovenia.

[24] Brunet, J. C. Poncet, A., and Trilhe, P., (1994), "Leak-Tightness Assessment of Demountable Joints for the Super Fluid Helium System of the CERN Large Hadron Collider (LHC)," Adv. Cryog. Eng., **39**, pp. 657–662.

[25] Beck, J. V., and Arnold, K. J., 1976, *Parameter Estimation in Engineering and Science*, Wiley, New York.

[26] Zimmerman, R. W., Kuzar, S., and Bodvarsson, G. S., 1991, "Lubrication Theory Analysis of the Permeability of Rough-Walled Fractures," Int. J. Rock Mech. Min. Sci. Geomech. Abstr., **28**(4), pp. 325–331.

[27] Prat, M., Plouraboué, F., and Letalleur, N., 2002, "Averaged Reynolds Equation for Flow Between Rough Surfaces in Sliding Motion," Transp. Porous Media, **48**, pp. 291–313.

[28] Geoffroy, S., and Prat, M., 2004, "On the Leak Through a Spiral-Groove Metallic Static Ring Gasket," ASME J. Fluids Eng., **126**(1), pp. 48–54.